Journal of
Manufacturing and Materials Processing

MDPI

Article

Studies on the Effect of Laser Shock Peening Intensity on the Mechanical Properties of Wire Arc Additive Manufactured SS316L

Geethapriyan Thangamani [1], Santosh Kumar Tamang [2], Md Saad Patel [3], Jinoop Arackal Narayanan [4,*], Muthuramalingam Thangaraj [5], Jufan Zhang [6], Pardeep Kumar Gianchandani [1] and Palani Iyamperumal Anand [7]

1 Department of Applied Science and Technology (DISAT), Politecnico Di Torino, Corso Duca degli Abruzzi 24, 10129 Torino, Italy; devimani.priyan18@gmail.com (G.T.); pardeep.gianchandani@polito.it (P.K.G.)
2 Department of Mechanical Engineering, North Eastern Regional Institute of Science and Technology, Nirjuli 791109, Arunachal Pradesh, India; skt@nerist.ac.in
3 School of Mechanical Engineering, Vellore Institute of Technology, Vellore 632014, Tamil Nadu, India; mdsaad.patel@vit.ac.in
4 Department of Engineering, School of Computing, Engineering and Digital Technologies, Teesside University, Middlesbrough TS1 3BX, UK
5 Department of Mechatronics Engineering, SRM Institute of Science and Technology, Kattankulathur, Chengalpattu 603203, Tamil Nadu, India; muthurat@srmist.edu.in
6 School of Mechanical and Materials Engineering, University College Dublin, Belfield, D04 V1W8 Dublin, Ireland; jufan.zhang@ucd.ie
7 Mechatronics and Instrumentation Laboratory, Department of Mechanical Engineering, Indian Institute of Technology Indore, Indore 453552, India; palaniia@iiti.ac.in
* Correspondence: anjinoop@gmail.com

Abstract: This study examines the impact of laser shock peening (LSP) on the mechanical properties, microstructural features, and elemental distribution of stainless steel 316L (SS316L) produced using wire arc additive manufacturing (WAAM). The investigation focuses on significant changes in mechanical behavior, surface topography, and porosity following LSP treatment, comparing these results to the untreated condition. LSP treatment significantly enhanced the ultimate tensile strength (UTS) and yield strength (YS) of WAAM-fabricated SS316L samples. The UTS of the as-manufactured WAAM specimen was 548 MPa, which progressively increased with higher LSP intensities to 595 MPa for LSP-1, 613 MPa for LSP-2, and 634.5 MPa for LSP-3, representing a maximum improvement of 15.8%. The YS showed a similar trend, increasing from 289 MPa in the as-manufactured specimen to 311 MPa (LSP-1) and 332 MPa (LSP-2), but decreasing to 259 MPa for LSP-3, indicating over-peening effects. Microstructural analysis revealed that LSP induced severe plastic deformation and reduced porosity from 14.02% to 4.18%, contributing to the improved mechanical properties. Energy dispersive spectroscopy (EDS) analysis confirmed the formation of an oxide layer post-LSP, with an increase in carbon (C) and oxygen (O) elements and a decrease in chromium (Cr) and nickel (Ni) elements on the surface, attributed to localized pressure and heat impacts. LSP-treated samples exhibited enhanced mechanical performance, with higher tensile strengths and improved ductility at higher laser intensities. This is due to LSP effectively enhancing the mechanical properties and structural integrity of WAAM-fabricated SS316L, reducing porosity, and refining the microstructure. These improvements make the material suitable for critical applications in the aerospace, automotive, and biomedical fields.

Keywords: wire arc additive manufacturing (WAAM); laser shock peening (LSP); stainless steel (SS316L); mechanical performance; fractography analysis

Received: 19 November 2024
Revised: 13 December 2024
Accepted: 28 December 2024
Published: 30 December 2024

Citation: Thangamani, G.; Kumar Tamang, S.; Patel, M.S.; Arackal Narayanan, J.; Thangaraj, M.; Zhang, J.; Kumar Gianchandani, P.; Iyamperumal Anand, P. Studies on the Effect of Laser Shock Peening Intensity on the Mechanical Properties of Wire Arc Additive Manufactured SS316L. *J. Manuf. Mater. Process.* **2025**, *9*, 8. https://doi.org/10.3390/jmmp9010008

1. Introduction

The rapid development of additive manufacturing (AM) technology has transformed the manufacturing process of complex and large-scale metal components, providing unparalleled design flexibility, material efficiency, and shorter lead times. Among these methods, wire arc additive manufacturing (WAAM) is notable for its capacity to produce large and complex metal components as it offers several advantages, including a high deposition rate, efficient material utilization, and low-cost [1]. WAAM uses an arc welding process, such as gas metal arc welding (GMAW), to liquefy a metallic wire and gradually deposit it layer-wise to create the desired shape. This technology offers several advantages over traditional manufacturing procedures, including reduced material waste, shorter production times, and the capacity to make parts that are close to their ultimate shape [2]. Stainless steel 316L (SS316L) is a widely used material in various industries due to its excellent corrosion resistance, robust mechanical qualities, and weldability. WAAM has been successfully used to produce SS316L components for application in the aerospace, automotive, biomedical, and marine industries [3]. Nevertheless, the WAAM fabricated parts occasionally have poor mechanical properties when compared to their fabricated counterparts (traditional processes like casting and secondary processing, which involve rolling and forging to fabricate SS316L components). The primary reason for this is the process core features, which include rapid cooling, step-by-step material deposition, and the formation of columnar grains [4]. These factors can cause residual stresses, changes in microstructure, and anisotropy, which can have a negative impact on the mechanical properties of manufactured components. Several post-processing approaches have been explored by the researchers to solve these limitations and improve the mechanical properties of SS316L manufactured by WAAM. The procedures described include heat treatment, hot isostatic pressing (HIP), laser shock peening (LSP), and mechanical surface treatments [5]. LSP has proven to be a very promising technology for improving the mechanical properties of metallic components. It is a surface modification method that uses high-energy laser intensity to blast material surfaces. The pulses generate shock waves, which cause compressive residual stresses (CRSs) and improve the microstructure of the material [6]. The narrative on WAAM of SS316L contains several major findings about microstructural evolution and mechanical behavior.

Chen et al. [7] examined the microstructure and room temperature tensile characteristics of GMAW-AM 316L and discovered that the microstructure consists of austenite (γ), delta-ferrite (δ), and sigma (σ) phases. The tensile characteristics of GMAW-AM 316L steel were comparable to wrought 316L and exceeded industry specifications. The presence of dimples on the fracture surface indicated a ductile fracture. As the volume percentage of the σ phase grew, the microhardness also increased. Similarly, Wang et al. [8] reported the effects of several arc modes on the microstructure and mechanical properties of WAAM-fabricated SS316L. It was reported that the grain orientations are in the building direction, indicating an austenite and ferrite microstructure. Additionally, the arc mode determined the mechanical properties, with different modes providing varying tensile and yield strengths. Thangamani et al. [9] investigated the improvement of the corrosion resistance and mechanical characteristics of stainless steel 308L made with WAAM by using LSP. The investigation demonstrated enhancements in compressive strength and corrosion resistance alongside a decrease in surface roughness and a transition from hydrophilic to hydrophobic surfaces after LSP. The study highlighted that grain refinement and elevated dislocation density resulting from LSP improve the material's overall performance, especially regarding compressive strength and passive film development for enhanced corrosion resistance. Ge et al. [10] studied the microstructural evolution and mechanical characteristics of a 2Cr13 steel thin-wall part produced with CMT-WAAM. They discovered a spatial periodicity of martensite laths within the block-shaped ferrite matrix in the

inner layers. Mechanical qualities (microhardness and tensile strength) were discovered to be influenced by the location's temperature history and microstructure. Rodrigues et al. [11] created a 316L stainless steel/Inconel 625 functionally graded material (FGM) using T-WAAM and two deposition strategies: (A) direct interface (FGM 100-100) and (B) smooth interface (FGM 5). The study indicated that the direct interface technique does not produce secondary phases, resulting in better mechanical characteristics and lower residual stress. The FGM produced with direct interface had an average strength of 542 MPa and elongation of 61.6%, whereas smooth interface exhibited a lower strength of 503 MPa and elongation of 32.4%. The fractures in the direct and smooth-type transitions occurred at 50 and 65 wt.% stainless steel regions, respectively.

Gowthaman et al. [12] investigated the impact of heat input on the microstructure and mechanical properties of SS316L produced using CMT-WAAM. It was discovered that the microstructure was composed of equiaxed and columnar grains, and the grain size varied with heat input. Heat input also affects the tensile parameters such as UTS, YS, and elongation. The samples with a travel speed (TS) of 4.1 m/min and a wire feed speed (WFS) of 4.8 m/min had the highest UTS (459.3 MPa), YS (277.5 MPa), and elongation (39%). Sabzi et al. [13] studied how continuous and pulsed current modes in the gas tungsten arc welding (GTAW) process affected the microstructure, mechanical characteristics, and fracture mechanism of dissimilar welded joints of AISI 316L and AISI 310S stainless steels utilizing ER309L filler metal. The results showed that the pulsed current mode resulted in finer equiaxed dendrites, lower delta ferrite content, and higher microhardness and Charpy impact toughness than the continuous current mode. The hardness values in the center of the WM in welded joints made from continuous and pulsed currents were 249 $\pm$ 8 and 315 $\pm$ 9 HV, respectively. Amiri [14] fabricated a FGM from plain carbon steel, SS316L, and Inconel 625 utilizing WAAM. The microstructure of SS316L was ferrite-austenite with delta ferrite, whereas Inconel 625 had Laves phase development. The hardness values for Inconel 625, SS316L, and plain carbon steel were 194–257 HV, 171–178 HV, and 159–170 HV, respectively. The FGM had a UTS of 487 $\pm$ 10 MPa, YS of 300 $\pm$ 6 MPa, and elongation of 40% $\pm$ 0.15. Haden et al. [15] evaluated the mechanical and wear performance of wire-based WAAM deposition of steel metals, namely SS304 and mild steel ER70S. Graded material properties of stainless steel 304 were observed for wear and hardness in the direction of deposition and Z height, owing to differences in the metal's local thermal histories. Wear rates decreased significantly, and microhardness values increased significantly. Rafieazad et al. [16] used WAAM with surface tension transfer (STT) to create an ER70S-6 low-carbon, low-alloy steel wall. The microstructure was composed of fine polygonal ferrite, lamellar pearlite, bainite, and acicular ferrite. Tensile strength was equivalent horizontally and vertically (~400 MPa yield strength and ~500 MPa ultimate tensile strength), but elongation was three times higher horizontally due to anisotropy in ductility. The lower vertical ductility was attributed to coarser grains, brittle martensite-austenite components, and discontinuities in the interpass areas.

Past research has highlighted the important relationship between processing parameters, microstructural changes, and the mechanical characteristics of SS316L components produced by WAAM. By manipulating process settings and employing proper post-processing techniques, it is possible to enhance the mechanical properties and minimize the anisotropy in components produced through additive manufacturing [17].

This work attempts to investigate the application of LSP as a post-processing method for WAAM-manufactured SS316L, with a novel focus on improving its microstructure, fractographic behavior, and tensile properties. This work analyzes in a novel way how LSP enhances tensile strength, yield strength, and ductility in SS316L, in contrast to previous research that focuses on compressive strength and corrosion resistance, especially in SS308L.

the addition, it fills the gaps in the existing literature on additive manufacturing by offering fresh perspectives on porosity reduction and grain refining after LSP.

2. Materials and Methods

The WAAM technique was carried out using a 1.2 mm SS316L wire. The chemical composition of the wire is presented in Table 1. The GMAW machine was used to deposit it on a mild steel (MS) base with dimensions of 100 × 100 × 10 mm. The optimal processing parameters are reported in Table 2. Argon was used as a shielding gas throughout the process with a nominal flow rate of 20 l/min, and the torch angle was kept at 90° with respect to the base. Figure 1a shows a schematic of the complete process; 50 layers (approximately 145 mm in height and 10 mm in bead width) were deposited to construct thin-walled structures, as shown in Figure 1b–d. The processing was done in an open atmosphere, resulting in surface oxidation of the built structures, as seen in Figure 1. To characterize and test the newly developed SS316L thin wall structures, consistent samples were extracted using the wire electric discharge machining process.

Table 1. Chemical composition of SS316L wire.

Elements	Fe	Cr	Ni	Mo	Mn	Si	N	C	S	O
Weight %	62.58	16.47	9.25	1.62	1.78	0.53	1.67	2.04	0.26	3.81

Table 2. Detailed process parameters for SS316L WAAM fabrication.

Process Parameters	Voltage (V)	Arc Length (mm)	Scanning Speed (mm/s)	Gas Flow Rate (L/min)	Stand-Off Distance (mm)
SS316L	17.5	0.8	91.67	20	20

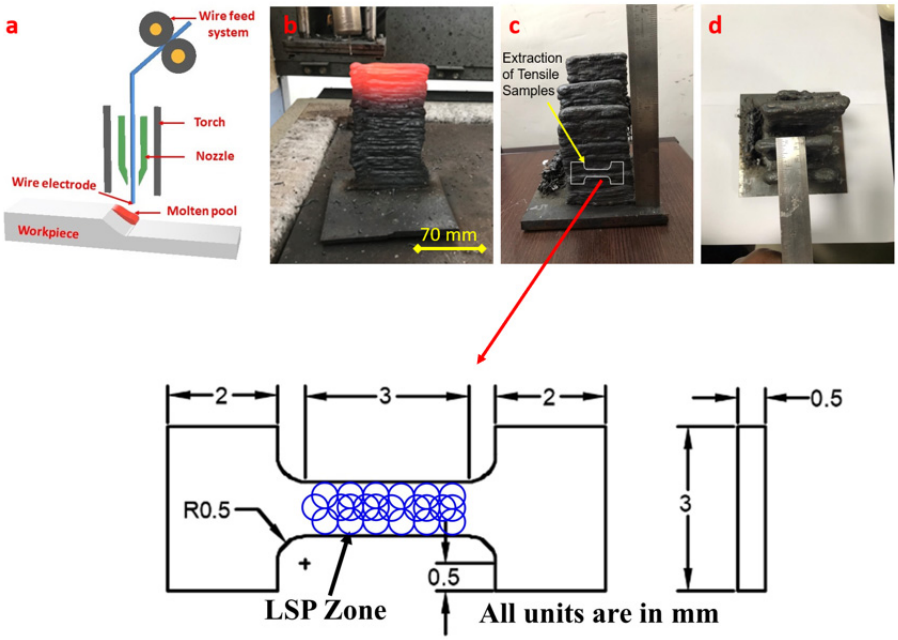

Figure 1. (**a**) Schematic diagram of WAAM; (**b**) 50-layer deposition; (**c**) 145 mm in height; and (**d**) 10 mm in length and width.

This study used a Q-Switched Nd:YAG pulse laser (Litron laser, Model: LPY674G-10, Mode: Gaussian) with a 532 nm wavelength, 10 Hz repetition rate, 300 mJ pulse energy, 9 ns pulse duration, 0.8 mm spot diameter, and a 3 mm thick deionized water confinement layer.

The laser beam scanned a 10 × 10 mm square area with 50% overlap. The LSP procedure involved no sacrificial coating and was carried out at room temperature. Before testing, the samples were finely polished, and LSP was done on a surface with three impacts using the X-Y translation stage movement. Figure 2 shows a schematic depiction of laser-treated SS316L surfaces utilizing the LSP process. Variable process parameters for LSP treatment on WAAM SS316L samples are laser intensity: 5.3 GW/cm^2, 10.2 GW/cm^2, and 15 GW/cm^2 for LSP1, LSP2, and LSP 3, respectively. This study utilized a total of 12 samples, with 3 distinct samples for each of the four conditions: WAAM, LSP (1), LSP (2), and LSP (3). Each condition was tested in triplicate, resulting in a total of 12 samples across all experimental repetitions.

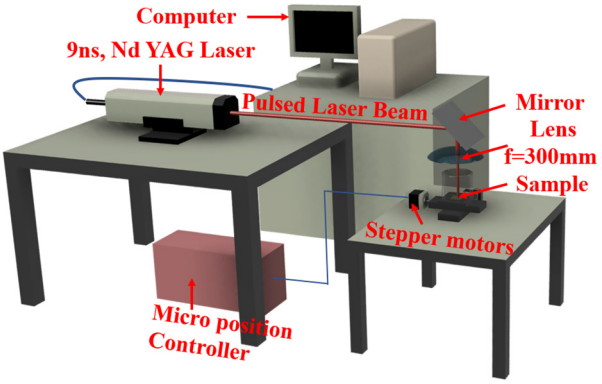

Figure 2. Schematic representation of the LSP technique.

A scanning electron microscope (SEM) equipped with energy-dispersive x-ray spectroscopy (EDS) (Make: Zeiss) was used to examine the microstructure. Samples for microstructural analysis were mechanically polished on a disc with (no. P200) emery sheets, then further polished with diamond paste to obtain a scratch-free surface. To expose the grain boundaries (GBs), the samples were chemically etched at room temperature for 20 s with a diluted aqua regia solution comprising 20 mL HCl, 10 mL HNO_3, and 30 mL deionized water. Porosity measurements were conducted using an optical microscope and analyzed with Dewinter Material Plus 4.5 software to evaluate the porosity percentage of both LSP-treated and untreated specimens. To evaluate the mechanical performance of the developed thin wall SS316L specimen micro-tensile testing was performed at room temperature with a crosshead velocity of 1 mm/min using a servo-hydraulic universal testing machine (UTM) with 10 kN load cell (model no: UT-04-0100, AGX-V). The detailed tensile specimen dimension is given in Figure 1. Before the examination, the specimens were thoroughly polished with fine emery sheets to maintain the consistency of the surface roughness. Fractography examination of tested specimens was performed using SEM to determine the cause of failure.

3. Results and Discussion

3.1. Topography

The SEM microstructure of WAAM SS316L is shown in Figure 3. It can be seen that, after cooling and solidification, the liquid stainless steel (SS) metal formed ferrites with a skeletal structure, which is an intrinsic feature of SS. Additionally, the GMAW approach used in the fabrication resulted in coarse residual ferrite with trivial porosity, which is evident in the micrographs as shown in Figure 3b. Reported microstructures are in line with the literature [18,19].

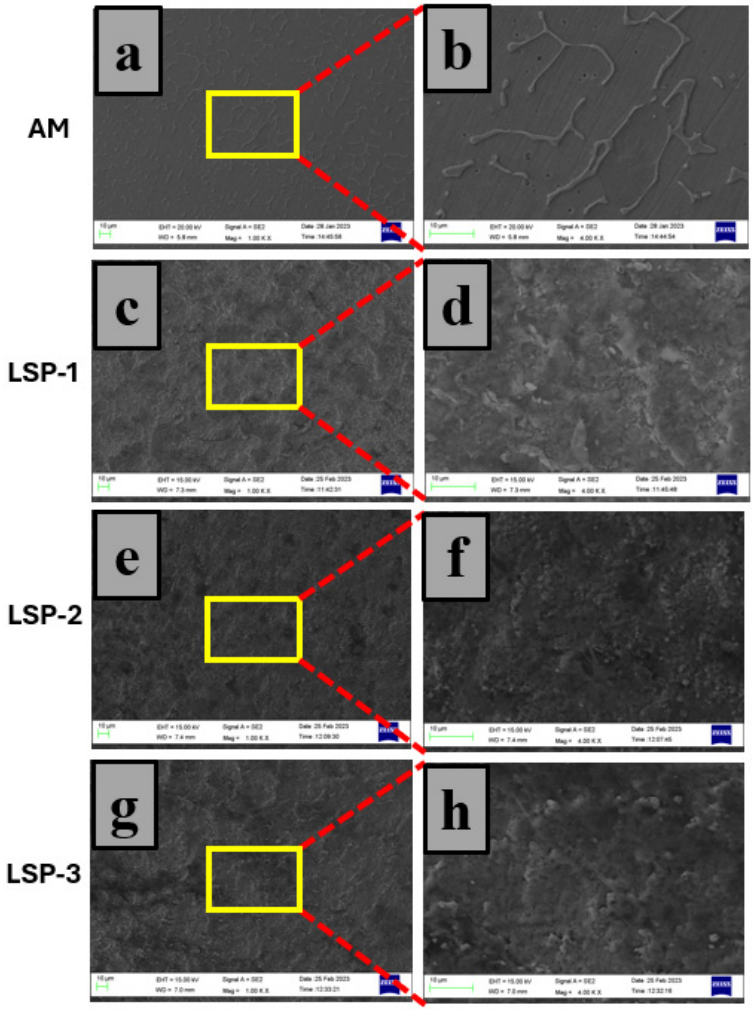

Figure 3. SEM micrographs showing the topography of WAAM-fabricated SS316L specimen (**a**,**b**) WAAM, (**c**,**d**) LSP-1, (**e**,**f**) LSP-2, (**g**,**h**) LSP-3.

After LSP, SEM analysis reveals the morphology of the LSP-treated specimen (Figure 3b–h). The surface layer is completely deformed following LSP, as pulsed lasers vaporize the specimen's ablation layer, resulting in plasma formation [20]. Water inhibits the plasma from expanding, resulting in a high-pressure shock wave at the target surface [21]. This high-pressure shock wave propagates into the target surface, inducing severe plastic deformation (SPD), as illustrated in Figure 3h, which results from the introduction of compressive residual stresses (CRSs) into the material [22,23]. The LSP process further breaks down the grains formed during the solidification of WAAM-fabricated SS316L. To refine a grain or cluster of grains, sufficient energy was applied once the laser beam's heat was delivered via a shock wave. The transmitted wave pressure causes significant plastic deformation of the grains, resulting in a refined grain boundary.

3.2. Element Distribution

Area EDS mapping was carried out to confirm the elemental composition before and after LSP treatment, as shown in Figure 4a–d. The area used for microstructural analysis in Figure 3 is used for EDS mapping. Chromium (Cr) and nickel (Ni) concentrations decreased as the laser intensity of LSP treatments increased, but carbon (C) and oxygen (O) levels increased as a result of the LSP process. Since LSP is a method that uses high-energy laser pulses to generate substantial heat and promote local surface oxidation, it increases the O content of the treated surface. Carbon contamination can also emerge from the

atmosphere or carbon-based residues on the substance's surface, which become more visible following LSP treatment. The severe localized pressure and heat impacts of LSP can cause the diffusion and redistribution of alloying elements like Cr and Ni. These elements migrate from the surface to the deeper regions, resulting in the depletion of the treated surface layer. This diffusion is driven by the higher laser intensity and stress fields induced by the LSP process [24].

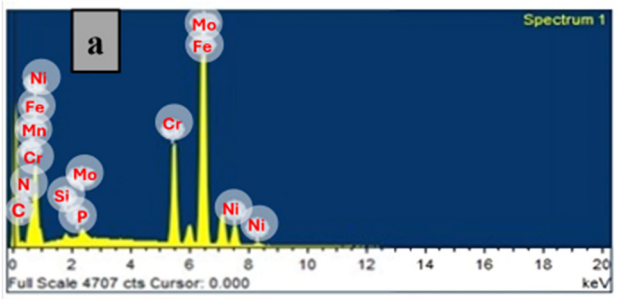

Element	Weight%	Atomic%
C K	4.39	17.05
N K	1.04	3.45
Si K	0.48	0.80
P K	0.18	0.26
Cr K	16.92	15.17
Mn K	1.64	1.39
Fe K	64.37	53.75
Ni K	9.01	7.15
Mo L	1.98	0.96
Totals	100.00	

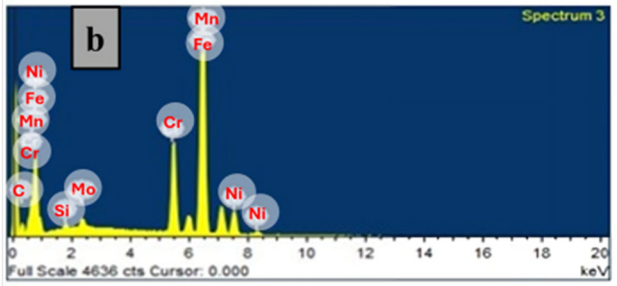

Element	Weight%	Atomic%
C K	9.72	33.28
Si K	0.53	0.78
Cr K	15.55	12.30
Mn K	1.72	1.29
Fe K	60.50	44.54
Ni K	9.89	6.93
Mo L	2.09	0.89
Totals	100.00	

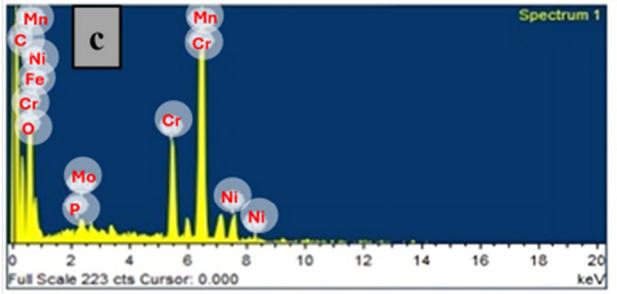

Element	Weight%	Atomic%
C K	29.53	52.62
O K	21.32	28.52
P K	0.07	0.05
Cr K	8.87	3.65
Mn K	0.84	0.33
Fe K	33.35	12.78
Ni K	4.99	1.82
Mo L	1.04	0.23
Totals	100.00	

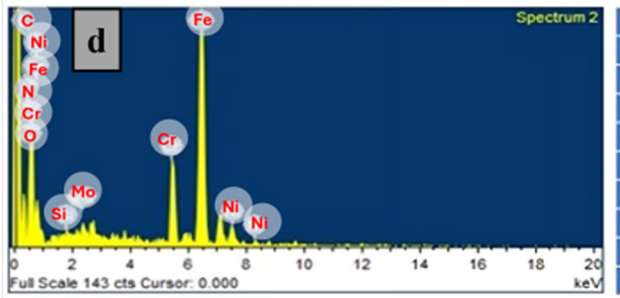

Element	Weight%	Atomic%
C K	37.21	57.17
N K	4.66	6.13
O K	21.32	24.60
Si K	0.09	0.06
Cr K	6.03	2.14
Fe K	26.35	8.71
Ni K	2.89	0.91
Mo L	1.45	0.28
Totals	100.00	

Figure 4. Area EDS analysis of WAAM fabricated SS316L specimen: (**a**) WAAM, (**b**) LSP-1, (**c**) LSP-2, (**d**) LSP-3.

3.3. Microstructural Analysis

Figure 5 displays the cross-sectional microstructural examination of AM and LSP-treated samples. It shows how the subsurface grains progressively refine as the laser intensity increases from LSP-1 to LSP-3. Cellular grain structure which is a characteristic feature of rapid solidification is observed in the WAAM sample. In LSP-1, shock waves cause plastic deformation, leading to grain refinement near the surface, as seen in Figure 5b. The increased laser intensity in LSP-2 and LSP-3 generates higher shock pressure, resulting in increased strain rates and promoting dynamic recrystallization. This leads to a further improvement in grain refinement, as evidenced in Figure 5c,d.

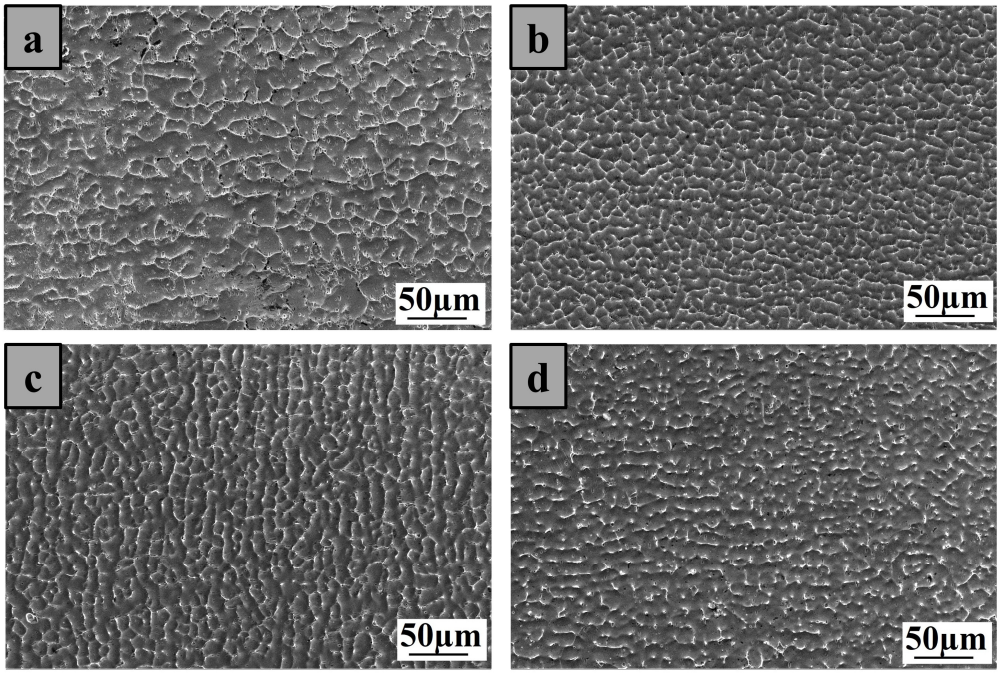

Figure 5. SEM microstructure of WAAM fabricated SS316L specimen: (**a**) WAAM, (**b**) LSP-1, (**c**) LSP-2, (**d**) LSP-3.

3.4. Porosity Measurement

The AM SS316L had a porosity of 14.02 (%), which is mainly due to variations in arc stability, wire travel speed, and heat input which creates a twirling motion in the liquid pool, trapping gases and resulting in the formation of pores in the fabricated thin walls [25]. Furthermore, extreme cooling rates can trap gases in the solidifying metal, particularly if the molten pool solidifies prematurely without allowing the gases to escape. Figure 6 shows how LSP reduced porosity to 4.18%. LSP uses high-energy laser pulses to generate shock waves, causing severe plastic deformation in the material. This deformation reduces microvoids and porosity, effectively compacting the material. Additionally, the localized thermal and mechanical impacts of LSP can improve the microstructure by decreasing the size and distribution of porosity throughout the WAAM process.

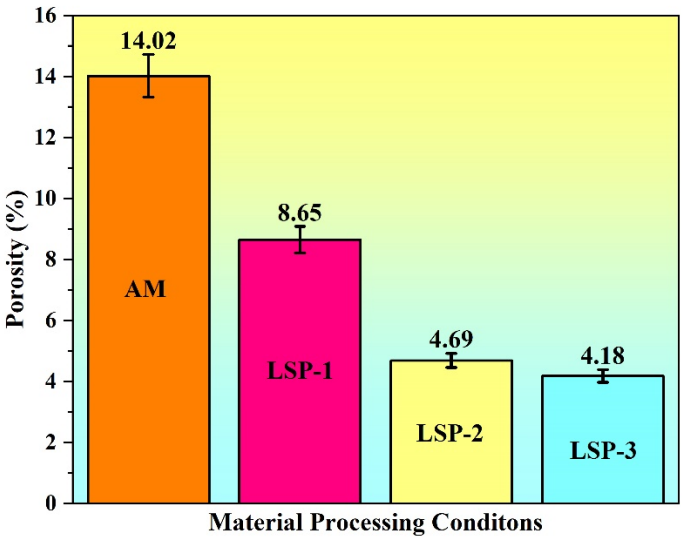

Figure 6. The porosity of WAAM fabricated SS316L samples for various processing conditions.

3.5. Mechanical Performance

Micro-tensile testing evaluates mechanical performance in miniature, localized areas impacted by LSP, revealing precise information about changes in microstructure and residual stress profiles. This approach can detect fine-scale changes in material behavior that macro testing may miss, such as LSP's impacts on grain boundaries, phase transformations, and micro-crack formation. Understanding the stress gradients caused by LSP via micro-tensile testing is critical for predicting the performance and reliability of treated components in service. Furthermore, it can identify changes in mechanical characteristics during the early stages of deformation, providing information about various fracture mechanisms involved. Table 3 and Figure 7 summarize the mechanical performance of material under various processing conditions.

Table 3. Micro-tensile performance results.

	YS (MPa)	UTS (MPa)	Elongation, ε (%)
WAAM	289 ± 8.5	548 ± 7	56.46 ± 5
LSP 1	311 ± 7.5	595 ± 8	56.54 ± 7
LSP 2	332 ± 7	613 ± 6	51.20 ± 6
LSP 3	259 ± 6.5	634.5 ± 6	59.71 ± 5

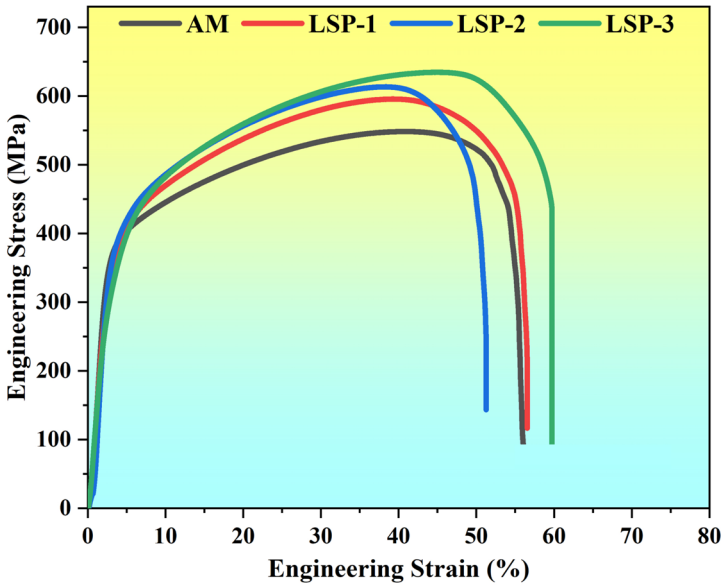

Figure 7. Stress vs. strain curve for WAAM fabricated SS316L specimen.

The yield strength (YS) of the micro-testing specimens shows notable variations upon LSP. The WAAM specimen has a YS of 289 MPa, with the application of LSP-1 increasing the YS to 311 MPa, representing a 7.6% improvement. Further enhancement is observed with LSP-2, which achieves the highest YS of 332 MPa, a 14.9% increase compared to the WAAM specimen. Conversely, LSP-3 results in a decrease in YS to 259 MPa, which is 10.4% lower than the AM specimen. The increase in YS for LSP-1 and LSP-2 can be attributed to the induced compressive residual stresses, reduced porosity, and refined microstructure due to the shock waves generated during peening. These compressive stresses hinder dislocation movement, thereby increasing the yield strength. The decrease in YS for LSP-3 might be due to over-peening, which can cause micro-cracks or excessive hardening, leading to a reduction in yield strength. Similar observations are reported in published literature [26,27].

The ultimate tensile strength (UTS) also improves with LSP treatment. The WAAM specimen exhibits a UTS of 548 MPa. LSP-1 increases the UTS to 595 MPa, an 8.6% improvement. LSP-2 further increases the UTS to 613 MPa, representing an 11.9% increase over the WAAM specimen. The most significant improvement is observed with LSP-3, achieving a UTS of 634.5 MPa, a remarkable 15.8% increase. The consistent improvement in UTS across all LSP conditions suggests that LSP effectively enhances the overall tensile properties of the material. The significant increase for LSP-3 indicates that, despite the decrease in YS, the material can withstand higher ultimate loads before fracture, likely due to work hardening and improved microstructural integrity. The elongation at fracture (ε) shows mixed results. The WAAM specimen has an elongation of 56.46%. LSP-1 results in a slight increase to 56.54%, indicating a negligible change. LSP2, however, reduces the elongation to 51.20%, a 9.3% decrease, suggesting a trade-off between strength and ductility. LSP-3, on the other hand, results in the highest elongation of 59.71%, a 5.8% increase compared to the AM specimen, indicating that LSP-3 not only improves strength but also enhances ductility. The variation in elongation among the different conditions highlights the balance between strength and ductility. LSP-1 maintains a similar elongation to the AM specimen, while LSP-2 shows a reduction, indicating that the increase in strength comes at the expense of ductility. LSP-3, however, enhances elongation at the cost of YS, suggesting that this peening condition optimally balances the competing effects of hardening and residual stress relaxation. The contrasting effects of the different LSP conditions on the mechanical properties underscore the importance of optimizing peening parameters to achieve the desired balance between strength and ductility. LSP-2 appears to offer the highest YS and UTS, making it suitable for applications requiring high strength. In contrast, LSP-3 provides the best combination of UTS and elongation, making it ideal for applications where both strength and ductility are crucial. The results are presented in Table 2.

Following micro-tensile testing, fractographic analysis was performed using SEM to determine the failure mode, the findings are presented in Figure 8. The fracture surfaces of the AM samples showed hard cleavage facets and non-uniform dimples (Figure 8a–c). The presence of cleavage phases indicated brittle fracture features, which reduced the material's YS. Additionally, the variability of the dimples indicates inhomogeneous plastic deformation, which negotiates mechanical performance. The LSP-1 samples exhibited shear dimples on the fracture surface with no visible cleavage segments as shown in Figure 8d–f. This homogeneity in dimple formation suggests a more ductile failure mechanism, which is associated with an increase in both YS and elongation. The absence of cleavage stages allowed for greater plastic deformation, which improved the overall mechanical characteristics of the LSP-1 samples. The fracture surface of the LSP-2 samples exhibited larger dimples as shown in Figure 8g–i. The formation of larger dimples results in reduced ductility when compared with LSP-1. This loss in ductility is attributed to the creation of microcracks or stress concentrators during the LSP process, which may have caused premature failure under tensile loading. The existence of these microstructural flaws most likely reduced the material's ability to withstand substantial plastic deformations, resulting in a drop in elongation. The LSP-3 samples showed fine dimples over the fracture surface presented in Figure 8j–l. Fine dimples imply a highly ductile failure mode caused by extensive plastic deformation. This fine dimple structure is mainly connected with excellent toughness and ductility, which improves the YS and elongation of LSP-3 samples [27].

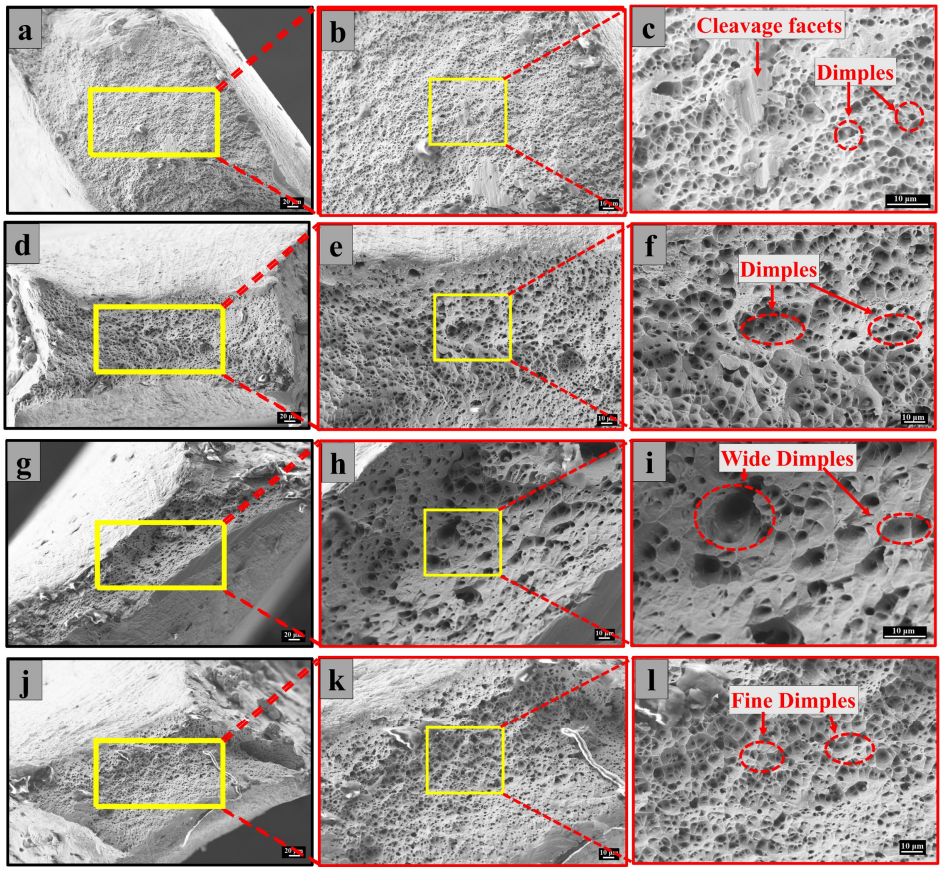

Figure 8. Fractography analysis of WAAM fabricated SS316L specimen: (**a**–**c**) AM, (**d**–**f**) LSP-1, (**g**–**i**) LSP-2, (**j**–**l**) LSP-3.

4. Conclusions

In the present study, the influence of LSP at various intensities on the microstructure and tensile characteristics of WAAM-fabricated SS316L alloy was evaluated. The key inferences of this work are summarized below:

1. The microstructure of the thin wall fabricated using GMAW-based WAAM revealed a skeletal-shaped colony of residual ferrite. The samples' surfaces showed severe plastic deformation after LSP treatment. Area EDS mapping confirmed the formation of the oxide layer after LSP with increasing C and O elements and decreasing Cr and Ni elements on the surface.
2. The high-energy laser pulses generated shock waves during LSP, causing severe plastic deformation and resulting in a reduction of porosity from 14.02% to 4.18%. This reduction is attributed to the compaction of material and the closure of microvoids due to the intense shock waves.
3. Micro-tensile studies indicate that increasing LSP intensities leads to increased strength and ductility. AM SS316L demonstrated a strength of 548 MPa and an elongation of 56.46%. The LSP-3 sample had the highest strength and ductility (634.5 MPa and 59.71%, respectively) among LSP-treated samples. This was primarily owing to refined microstructure and the induction of CRS, which hinders the dislocation movement and enhances the mechanical performance.
4. Fractographic analysis provided valuable insight into the failure modes of AM and LSP-treated samples. The AM samples had hard cleavage facets and non-uniform dimples, which indicated a mixed mode of fracture. In contrast, LSP samples exhibited dimple development and the absence of cleavage segments, which resulted in uniform

plastic deformation. LSP-3 samples had fine dimples, indicating extremely ductile failure with increased strength (UTS = 634.5 MPa) and elongation (%ε= 59.71%)

This study lays the foundation for enhancing the mechanical strength and customizing the surface properties of WAAM-built large-scale structures, particularly for applications in storage tanks within the aerospace and nuclear industries. The practical utility of the process can be further optimized by employing higher laser energy and a larger beam coverage area for peening large-scale structures. Future work will focus on investigating the influence of LSP parameters on the microstructural behavior at the nanoscale, grain texture, and residual stress. Additionally, studies will be conducted to examine the effects of LSP on the hardness and corrosion resistance of the samples.

Author Contributions: Conceptualization, G.T.; methodology, G.T.; validation, G.T., S.K.T., M.S.P., M.T., J.Z. and P.K.G.; Formal analysis, G.T., S.K.T., M.S.P., J.A.N., M.T. and J.Z.; Investigation, G.T., S.K.T., M.S.P., J.A.N., M.T., J.Z. and P.K.G.; resources, P.I.A.; data curation, G.T.; writing—original draft, G.T., S.K.T., M.S.P., M.T., J.Z. and P.K.G.; writing—review and editing, G.T., S.K.T., J.A.N., M.T., J.Z., P.K.G. and P.I.A.; visualization, S.K.T., M.T., J.Z. and P.K.G.; supervision, P.I.A.; project administration, P.I.A.; Funding acquisition, P.I.A. All authors have read and agreed to the published version of the manuscript.

Funding: The authors thank SERB (PDF/2021/002326) for providing funding or financial support for carrying out the research work under the National Post Doctoral Fellowship scheme. Also, the authors gratefully acknowledge the characterization facilities provided by the Sophisticated Instrumentation Center (SIC), IIT Indore.

Data Availability Statement: The data presented in this study are available upon request from the corresponding author.

Conflicts of Interest: The authors declare no conflicts of interest.

References

1. Mishra, R.K.; Debnath, S.; Ravi, K. Wire arc additive manufacturing of stainless steel 316L: Microstructure, mechanical properties, and corrosion behavior. *J. Mater. Eng. Perform.* **2023**, *32*, 8109–8121.
2. Ding, J.; Colegrove, P.; Mehnen, J.; Ganguly, S.; Williams, S. Geometrical accuracy and dimensional precision assessment in wire and arc additive manufacture. *Int. J. Adv. Manuf. Technol.* **2015**, *81*, 357–368.
3. Wang, F.; Williams, S.; Colegrove, P.; Li, L. Microstructure and mechanical properties of wire and arc additive manufactured Ti-6Al-4V. *J. Alloys Compd.* **2018**, *741*, 1005–1015. [CrossRef]
4. Zhang, Y.; Chen, Z.; Liu, J.; Li, J. Effect of heat treatment on microstructure and mechanical properties of wire arc additive manufactured Inconel 718 alloy. *Mater. Sci. Eng. A* **2022**, *831*, 142456.
5. Hu, Y.; Kovacevic, R. *Laser Shock Peening: Theory and Applications*; Elsevier: Amsterdam, The Netherlands, 2013.
6. Gujba, A.K.; Medraj, M. Laser shock peening: A review. *J. Mater. Process. Technol.* **2014**, *214*, 2932–2943.
7. Chen, X.; Li, J.; Cheng, X.; He, B.; Wang, H.; Huang, Z. Microstructure and mechanical properties of the austenitic stainless steel 316L fabricated by gas metal arc additive manufacturing. *Mater. Sci. Eng. A* **2017**, *703*, 567–577. [CrossRef]
8. Wang, C.; Liu, T.G.; Zhu, P.; Lu, Y.H.; Shoji, T. Study on microstructure and tensile properties of 316L stainless steel fabricated by CMT wire and arc additive manufacturing. *Mater. Sci. Eng. A* **2020**, *796*, 140006. [CrossRef]
9. Geethapriyan, T.; Palani, I.A.; Singh, M.K.; Rai, D.K.; Priyan, V.G.S.; Subbu, S.K. Post-processing of Wire Arc Additive Manufactured Stainless Steel 308L to Enhance Compression and Corrosion Behavior using Laser Shock Peening Process. *J. Mater. Eng. Perform.* **2024**, *33*, 9267–9281. [CrossRef]
10. Ge, J.; Lin, J.; Lei, Y.; Fu, H. Location-Related Thermal History, Microstructure, and Mechanical Properties of Arc Additively Manufactured 2Cr13 Steel Using Cold Metal Transfer Welding. *Mater. Sci. Eng. A* **2018**, *715*, 144–153. [CrossRef]
11. Gowthaman, P.S.; Jeyakumar, S.; Sarathchandra, D. Effect of Heat Input on Microstructure and Mechanical Properties of 316L Stainless Steel Fabricated by Wire Arc Additive Manufacturing. *J. Mater. Eng. Perform.* **2023**, *33*, 5536–5546. [CrossRef]
12. Sabzi, M.; Mousavi Anijdan, S.H.; Chalandar, A.R.B.; Park, N.; Jafarian, H.R.; Eivani, A.R. An experimental investigation on the effect of gas tungsten arc welding current modes upon the microstructure, mechanical, and fractography properties of welded joints of two grades of AISI 316L and AISI310S alloy metal sheets. *Mater. Sci. Eng. A* **2022**, *840*, 142877. [CrossRef]

13. Amiri, V.; Naffakh-Moosavy, H. Wire arc additive manufacturing of functionally graded carbon steel-stainless steel 316L-Inconel 625: Microstructural characterization and mechanical behavior. *J. Adv. Join. Process.* **2024**, *9*, 100194. [CrossRef]
14. Haden, C.V.; Zeng, G.; Carter III, F.M.; Ruhl, C.; Krick, B.A.; Harlow, D.G. Wire and arc additive manufactured steel: Tensile and wear properties. *Addit. Manuf.* **2017**, *16*, 115–123. [CrossRef]
15. Rafieazad, M.; Ghaffari, M.; Nemani, A.V.; Nasiri, A. Microstructural evolution and mechanical properties of a low-carbon low-alloy steel produced by wire arc additive manufacturing. *Int. J. Adv. Manuf. Technol.* **2019**, *105*, 2121–2134. [CrossRef]
16. Senthil, T.S.; Ramesh Babu, S.; Puviyarasan, M.; Dhinakaran, V. Mechanical and microstructural characterization of functionally graded Inconel 825-SS316L fabricated using wire arc additive manufacturing. *J. Mater. Res. Technol.* **2021**, *15*, 661–669. [CrossRef]
17. Vora, J.; Parmar, H.; Chaudhari, R.; Khanna, S.; Doshi, M.; Patel, V. Experimental investigations on mechanical properties of multi-layered structure fabricated by GMAW-based WAAM of SS316L. *J. Mater. Res. Technol.* **2022**, *20*, 2748–2757. [CrossRef]
18. Sasikumar, C.; Oyyaravelu, R. Mechanical properties and microstructure of SS 316 L created by WAAM based on GMAW. *Mater. Today Commun.* **2024**, *38*, 107807. [CrossRef]
19. Hareharen, K.; Kumar, P.; Panneerselvam, T.; Babu, D.; Sriraman, N. Investigating the effect of laser shock peening on the wear behaviour of selective laser melted 316L stainless steel. *Opt. Laser Technol.* **2023**, *162*, 109317. [CrossRef]
20. Radziejewska, J.; Strzelec, M.; Ostrowski, R.; Sarzyński, A. Experimental investigation of shock wave pressure induced by a ns laser pulse under varying confined regimes. *Opt. Lasers Eng.* **2020**, *126*, 105913. [CrossRef]
21. Sandmann, P.; Keller, S.; Kashaev, N.; Ghouse, S.; Hooper, P.A.; Klusemann, B.; Davies, C.M. Influence of laser shock peening on the residual stresses in additively manufactured 316L by Laser Powder Bed Fusion: A combined experimental–numerical study. *Addit. Manuf.* **2022**, *60*, 103204. [CrossRef]
22. Abeens, M.; Muruganandhan, R.; Thirumavalavan, K. Effect of Low energy laser shock peening on plastic deformation, wettability and corrosion resistance of aluminum alloy 7075 T651. *Optik* **2020**, *219*, 165045. [CrossRef]
23. Wei, X.; Ling, X.; Zhang, M. Influence of surface modifications by laser shock processing on the acid chloride stress corrosion cracking susceptibility of AISI 304 stainless steel. *Eng. Fail. Anal.* **2018**, *91*, 165–171. [CrossRef]
24. Arana, M.; Ukar, E.; Rodriguez, I.; Iturrioz, A.; Alvarez, P. Strategies to reduce porosity in Al-Mg WAAM parts and their impact on mechanical properties. *Metals* **2021**, *11*, 524. [CrossRef]
25. Samuel, C.; Moganraj, A.; Swaroop, S.; Praveenkumar, K.; Natarajan, A.; Rao, M.N.; Syed, B.; Bhattacharya, B. Effect of Laser Shock Peening without Coating on Grain Size and Residual Stress Distribution in a Microalloyed Steel Grade. *Crystals* **2023**, *13*, 212. [CrossRef]
26. Wang, Y.; Pan, X.; Wang, X.; Liu, Z.; Liu, S.; Wan, W.; Wang, P. Influence of laser shock peening on surface integrity and tensile property of high strength low alloy steel. Chinese. *J. Aeronaut.* **2021**, *34*, 199–208. [CrossRef]
27. Das, A.; Tarafder, S. Geometry of dimples and its correlation with mechanical properties in austenitic stainless steel. *Scr. Mater.* **2008**, *59*, 1014–1017. [CrossRef]